

COMPUTATION OF NORMAL IMPINGING JETS IN CROSS-FLOW AND COMPARISON WITH EXPERIMENT

K. KNOWLES AND D. BRAY

Aeromechanical Systems Group, Royal Military College of Science, Shrivenham, Swindon, Wiltshire SN6 8LA, U.K.

SUMMARY

The PHOENICS code has been used to model the flow field surrounding subsonic and underexpanded jets impinging on a ground plane in the presence of a cross-flow, for cases with both a fixed ground plane and a 'rolling road'. The standard $k-\epsilon$ turbulence model is used, without correction factors. It is confirmed that this overpredicts the free jet entrainment rate; the wall jet spreading rate is slightly underpredicted but the initial thickness is too high. Agreement with experiment is, nevertheless, much better than for previous calculations, showing the importance of the extent of the grid used. The ground vortex formed in cross-flow is shown to move with varying effective velocity ratio and with rolling road operation in the same manner as experimentally observed. Ground vortex self-similarity is also accurately predicted with the numerical modelling.

KEY WORDS Jets Vortex flows $k-\epsilon$ model Finite volume

1. INTRODUCTION

When a jet impinges on a surface normal to its axis, a wall jet is formed which spreads out radially from the impingement point. If a cross-flow (parallel to the wall) exists, the wall jet will eventually stagnate and roll up to form a vortex, arranged as a horseshoe about the jet (see Figure 1). This flow field is of particular interest in the development of V/STOL aircraft, where the cross-flow may be due to ambient wind or aircraft motion.

The position and strength of the ground vortex are important owing to their effect on aircraft pressure loads and air intake flows (where there is the specific problem of hot gas ingestion). Some of the factors which affect ground vortex position have been investigated previously, but there is considerable scatter in the experimental data and very little high-jet-Mach-number data.¹ The present project has looked at the influence of nozzle height, nozzle pressure ratio and cross-flow-to-jet velocity ratio with both fixed and moving ground planes (simulating ambient wind or aircraft motion). Details of the experimental work are given elsewhere.²

Numerical modelling of this flow field has been undertaken using the commercially available PHOENICS code. This well-known computational fluid mechanics package has been used before in similar flow fields to ours,³ but there do not appear to be published comparisons with experiments for the more complex jet flow fields, nor moving ground results. For the present work the modelling was developed from a simple round free jet through an axisymmetric impinging jet to a 2D impinging jet in cross-flow. These cases will each be discussed in turn, but first the numerical basis of the PHOENICS code will be described briefly.

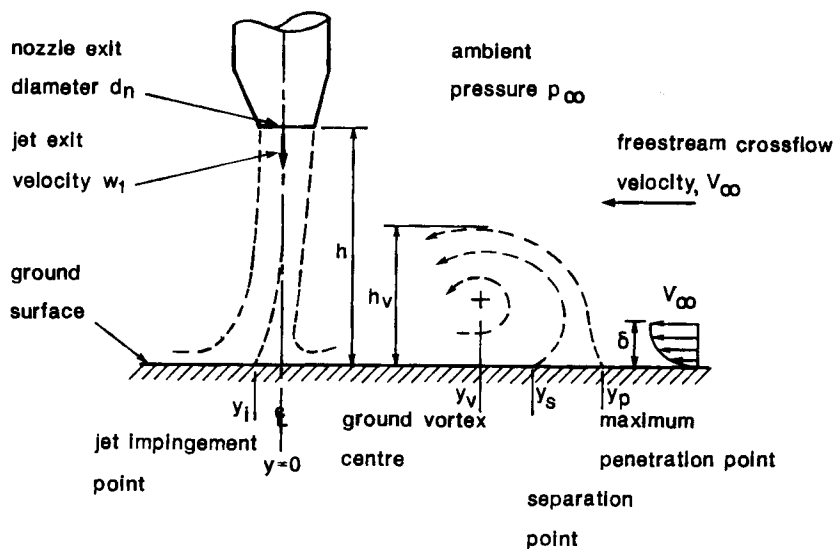


Figure 1. Impinging jet in cross-flow

2. NUMERICAL METHOD

PHOENICS uses a finite volume formulation of the differential equations of conservation involving mass, momentum, energy and turbulence quantities. The finite volume equations are derived by integration of the differential equations over control volumes (cells) which are of finite size.

The general, single-phase, three-dimensional, steady state conservation equations to be solved may be written as

$$\text{div}(\rho \mathbf{u} \phi + \mathbf{J}_\phi) = S_\phi, \quad (1)$$

where ϕ is the dependent variable, ρ is the density, \mathbf{u} is the vector velocity, \mathbf{J}_ϕ is the diffusive velocity vector and S_ϕ is the source of ϕ per unit volume. The variables solved for in this work are: v and w , the velocity components along the y - and z -axes respectively; k , the turbulent kinetic energy; and ε , the rate of dissipation of k . The pressure p does not appear explicitly as the subject of a conservation equation but is deduced from the continuity equation.

The derived set of linked equations is then solved in an iterative manner using a derivative of the SIMPLE algorithm,⁴ which is an implicit scheme. In this work, only steady state solutions are obtained. The whole field solution procedure was used (except for some of the free jet calculations).

Turbulence modelling was achieved by using the k - ε two-equation turbulence model. Thus the eddy viscosity ν_t is computed from $\nu_t = C_\mu k^2 / \varepsilon$, where k is the turbulent kinetic energy, ε is the rate of dissipation of k and the unmodified empirical constant has a value $C_\mu = 0.09$. This is basically the high- Re form of the k - ε model. The dissipation rate ε is solved from the transport equation

$$D\varepsilon/Dt = (\partial/\partial x_i)[(\nu_t/\sigma_\varepsilon)d\varepsilon/dx_i] + C_{1\varepsilon}(\varepsilon/k)P_k - C_{2\varepsilon}\varepsilon^2/k, \quad (2)$$

where P_k is the rate of production of k and the standard empirical values for the constants are again used:

$$\sigma_\varepsilon = 1.314, \quad C_{1\varepsilon} = 1.44, \quad C_{2\varepsilon} = 1.92.$$

These standard values have been found in the past^{5,6} to give inaccurate results when used for flows such as axisymmetric jets and wall jets⁷—precisely the areas of interest here. The conventional remedy in both cases is to make two of the turbulence model constants functions of a suitable mean flow retardation parameter. It was not felt, however, that this added complexity was worthwhile for the present work, where the free jet distances involved are quite small. Further justification for this decision will be given when results of the present computational work are compared with experiments and with other numerical results.

Adjacent to the wall the values of k and ϵ are fixed to wall values. A logarithmic law-of-the-wall was used such that

$$U^+ = (1/K) \ln(Ey^+), \quad (3)$$

$$k_w = U_\tau^2 C_\mu^{-1/2}, \quad (4)$$

$$\epsilon_w = U_\tau^3 / Ky, \quad (5)$$

where $U^+ = U/U_\tau$, $U_\tau = (\tau_w/\rho)^{0.5}$, $y^+ = U_\tau y/\nu_1$, $K = 0.435$ (the von Karman constant), $E = 9.0$ (a roughness factor for a smooth wall) and ν_1 is the laminar coefficient of kinematic viscosity.

As well as developing the modelling complexity from that of a free jet, through an impinging jet to the required impinging jet in cross-flow, various other parameters were also developed along the way. The grid was modified in each case to assess the grid independence of the solution. Relaxation factors and initial field values were also modified as the modelling progressed.

3. RESULTS AND DISCUSSION

3.1. Free jet

Calculations were performed on a subsonic air jet of pressure ratio $pr_n = 1.05, 1.2$ and 1.25 . An axisymmetric polar grid was used which had the z -axis aligned with the nozzle centreline, the y -axis being radial. The grid extended in the z -direction to 7.5 nozzle diameters downstream of the nozzle exit (to tie up with subsequent impinging jet calculations) and 2.36 diameters upstream. The nozzle internal flow was not, however, modelled. The grid size which was finally adopted was 24×31 (y by z), with finer grid spacing across the jet, near the jet exit and parallel to the downstream boundary.

Uniform nozzle exit conditions were assumed with turbulence intensities (TINT) of 10%, 5%, 3% or 1% being input. Heavy relaxation of the solution procedure was found to be necessary in order to achieve convergence. Convergence was made more difficult with decreasing turbulence intensity and increasing pr_n . In fact, it was not possible to converge satisfactorily the case with $pr_n = 1.25$ and TINT = 1%. Results from the present work have been compared with the $pr_n = 1.25$ experimental data of Donaldson and Snedeker.⁸ This confirms that the spreading rate is overpredicted and that the overprediction increases with increasing turbulence intensity. Similarly, Rodi⁵ has shown an overprediction of spreading rate of about 25%. Figure 2 plots jet centreline velocity (w_c), non-dimensionalised by the nozzle exit value (w_{c1}), against axial position in nozzle diameters (d_n) and shows that increasing jet turbulence shortens the potential core. The experimental turbulence intensity is not known in this case but would be expected to be around 3%, in which case the velocity decay rate is overpredicted. Also shown in Figure 2 is the effect of nozzle pressure ratio. A decrease in nozzle pressure ratio from 1.25 to 1.05 consistently increases the axial velocity decay rate. This trend conflicts with the PHOENICS calculations of Glynn⁶ while agreeing with the experimental findings of Curtis.⁹

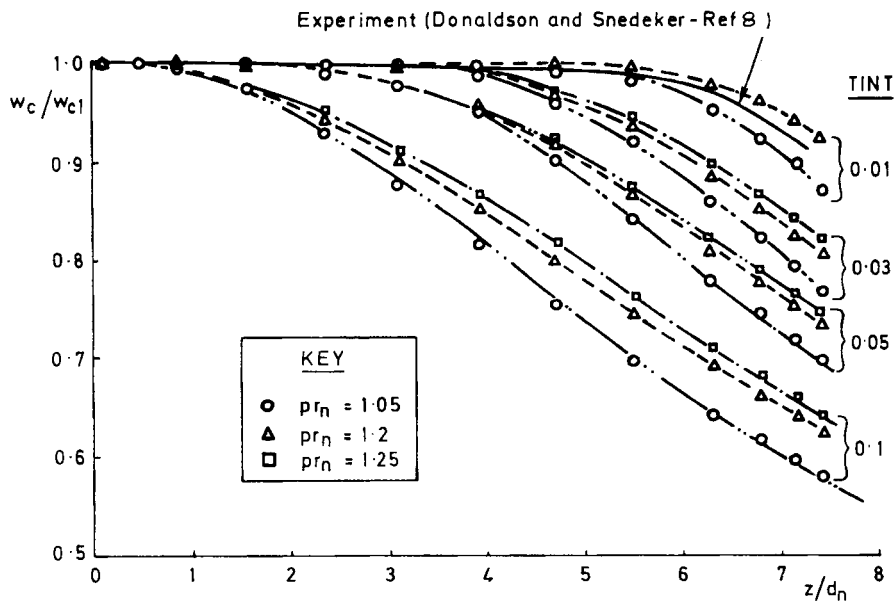


Figure 2. Subsonic free jet axial velocity decay—comparison between PHOENICS and experiment⁸

Before moving on to discuss impinging jets, it should be noted that for a turbulence intensity of 3% there is no underprediction of axial velocity within 4 diameters of nozzle exit and that at 7.5 diameters there is around a 9% underprediction. This is felt to be acceptable, for the time being, in the light of the jet lengths to be modelled for our V/STOL aerodynamics work.

3.2. Impinging jet

We now consider an axisymmetric air jet impinging on a plane normal to its axis, at a distance h . This produces three flow regimes: the free jet, the impingement region and the radial wall jet. Glauert¹⁰ studied the wall jet theoretically, Bakke¹¹ performed an empirical analysis whilst Poreh *et al.*¹² conducted extensive experiments and analysed previous work to show that

$$v_{wc} h' / \sqrt{KM} = 1.132 (y/h')^{-1.1}, \quad (6)$$

$$a_w/h' = 0.098 (y/h')^{0.9}, \quad (7)$$

where v_{wc} is the wall jet peak velocity, h' is the distance from the wall to the geometric origin of similarity of the jet, KM is the jet kinematic momentum flux ($\pi c d_n^2 w_{c1}^2/4$), c is the jet discharge coefficient, a_w is the wall jet thickness and y is the radial distance.

PHOENICS calculations for the impinging jet are relatively simple adaptations of the free jet cases. Again, a polar axisymmetric grid is used but extended in the radial (y) direction to $24.3d_n$. Five cases have been studied.

- Case 1. $h/d_n = 7.5$, $pr_n = 1.079$ (as for the experiments of Reference 12), 35×39 (z by y) grid, nozzle exit turbulence intensity (TINT) = 3%.
- Case 2. $h/d_n = 24$ (as for the experiments of Reference 12), 68×39 grid, otherwise as Case 1.
- Case 3. As Case 2 except for reduced turbulence intensity of 1%.
- Case 4. As Case 2 except for increased pr_n of 1.5.
- Case 5. As Case 2 except for $h/d_n = 5$.

Glynn and Jal⁶ have also studied an impinging jet using PHOENICS and made comparisons with the experimental data of Curtis.⁹ They used $h/d_n = 8.5$, $pr_n = 1.04$, 1.8 and 3.0, TINT = 1% and a 65×55 grid. Their principal finding was an underprediction of wall jet spreading, with the initial thickness being too great. This was probably caused, at least in part, by the inadequate extent of the y -axis, which was only $12d_n$. Standard turbulence model coefficients were used initially but then modified in line with References 5 and 7. This was found to give only small improvements in prediction accuracy.

Figures 3 and 4 compare PHOENICS results from the current work with those from Reference 6 and the experimental data of References 9 and 12.

3.3. Impinging jet in cross-flow

The flow field to be modelled is that sketched in Figure 1. To minimize core storage requirements, these initial calculations have been performed on an axisymmetric grid. This means that the jet cannot deflect in the cross-flow and that the free stream mass flow entering through the right-hand boundary must exit through the upper, free boundary. Over 40 cases have been modelled to date, with either a fixed ground plane or a rolling road moving at V_∞ .

The influence of the ground vortex can be seen by plotting the ground plane static pressure and the flow field velocity vectors as shown in Figure 5 for a typical case with $h/d_n = 10.0$, $V_g = 0$, $pr_n = 1.5$ and $V_\infty = 10.7 \text{ m s}^{-1}$. The minimum pressure lies under the vortex core; the forward penetration of the vortex is taken by some authors to be represented by $C_p = 0$, but for the present work y_p (see Figure 1) is taken as the position of (upstream) maximum C_p .

Experimental work¹³ has demonstrated a correlation between y_v , y_s and y_p which appears to be independent of other flow field parameters and therefore suggests a fixed ground vortex geometry

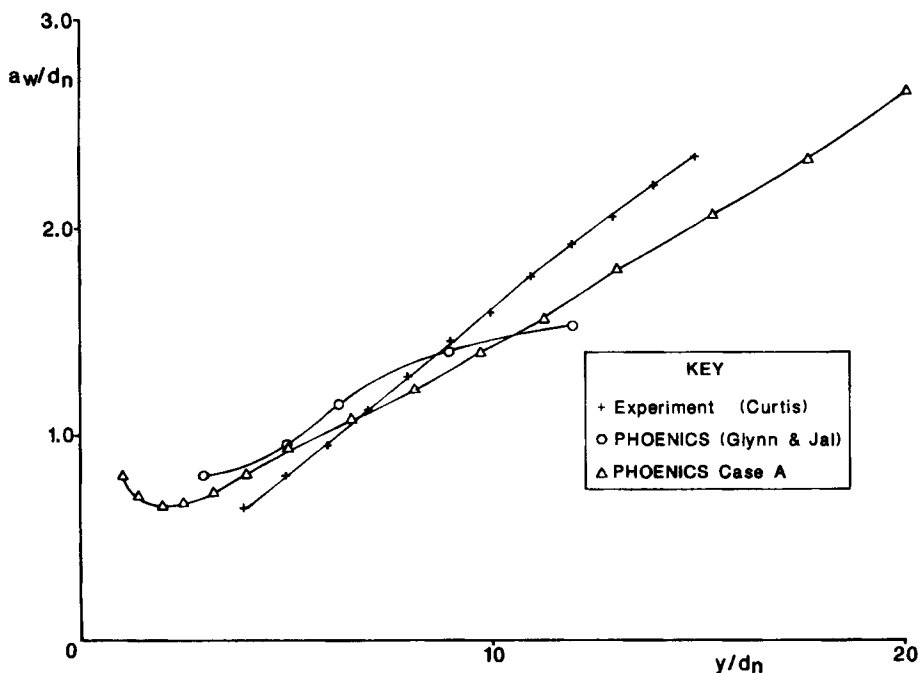


Figure 3. Wall jet spreading—comparison between PHOENICS and experiment⁹

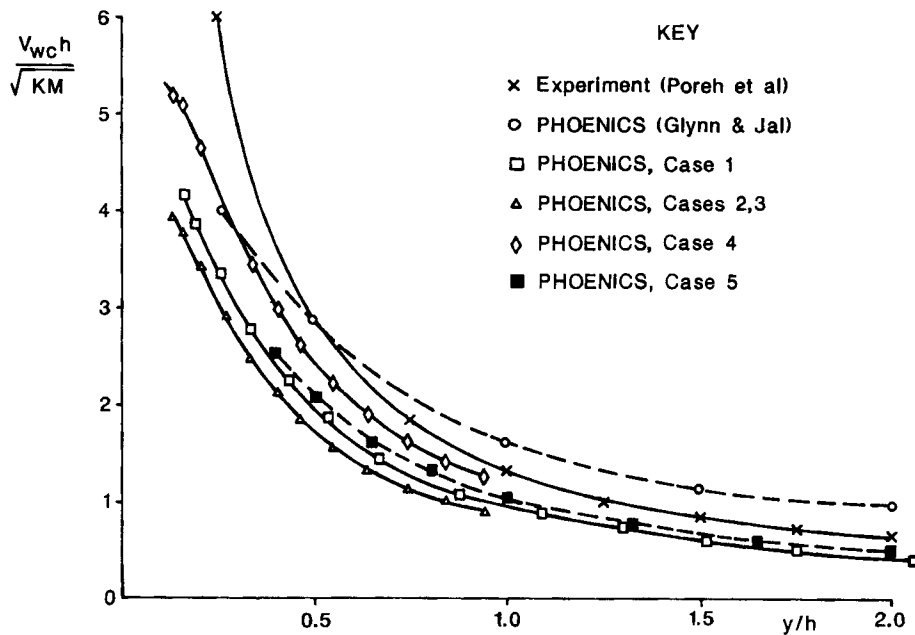


Figure 4. Wall jet decay rate—comparison between PHOENICS and experiment¹²

or self-similarity. Agreement between computation and experimentation is good (Figure 6), especially for the fixed relationship between y_s and y_p .

An important parameter determining the position of the ground vortex is the effective velocity ratio $V_e = (\rho_\infty V_\infty^2 / \rho_1 w_{c1}^2)^{0.5}$. Non-dimensional vortex penetration is plotted against this in Figure 7, where comparison is made with averaged experimental data of Reference 13. The averages here are taken over a range of pr_n and h/d_n . It can be seen that the computational modelling considerably overpredicts vortex separation distances by around $7d_n$. The overprediction is only to be expected from the 2D modelling constraints. These force all of the cross-flow out of the solution domain through the upper free surface boundary, thus detracting from the horizontal cross-flow momentum component which opposes the wall jet momentum. The trend of increasing separation distance with increasing V_e^{-1} is, however, correctly calculated numerically. The rate of increase is also predicted to a reasonably accurate degree.

The penetration reduction of the moving ground plane is shown in the numerical modelling, but with a predicted mean reduction of about half that measured experimentally. This is probably caused, at least in part, by the turbulence model inadequacies mentioned above. These lead to incorrectly predicted wall jet velocity profiles and therefore underpredicted wall jet shear stresses in moving ground plane operation.

4. CONCLUSIONS

It has been confirmed that using the standard $k-\epsilon$ turbulence model gives an overprediction of free jet spreading rate and an underprediction of wall jet spreading rate, with initial wall jet thickness being too great. For a free jet which is 7.5 nozzle diameters in length, however, this gives a peak velocity which is in error by less than 10%. Whilst the usual modifications to the

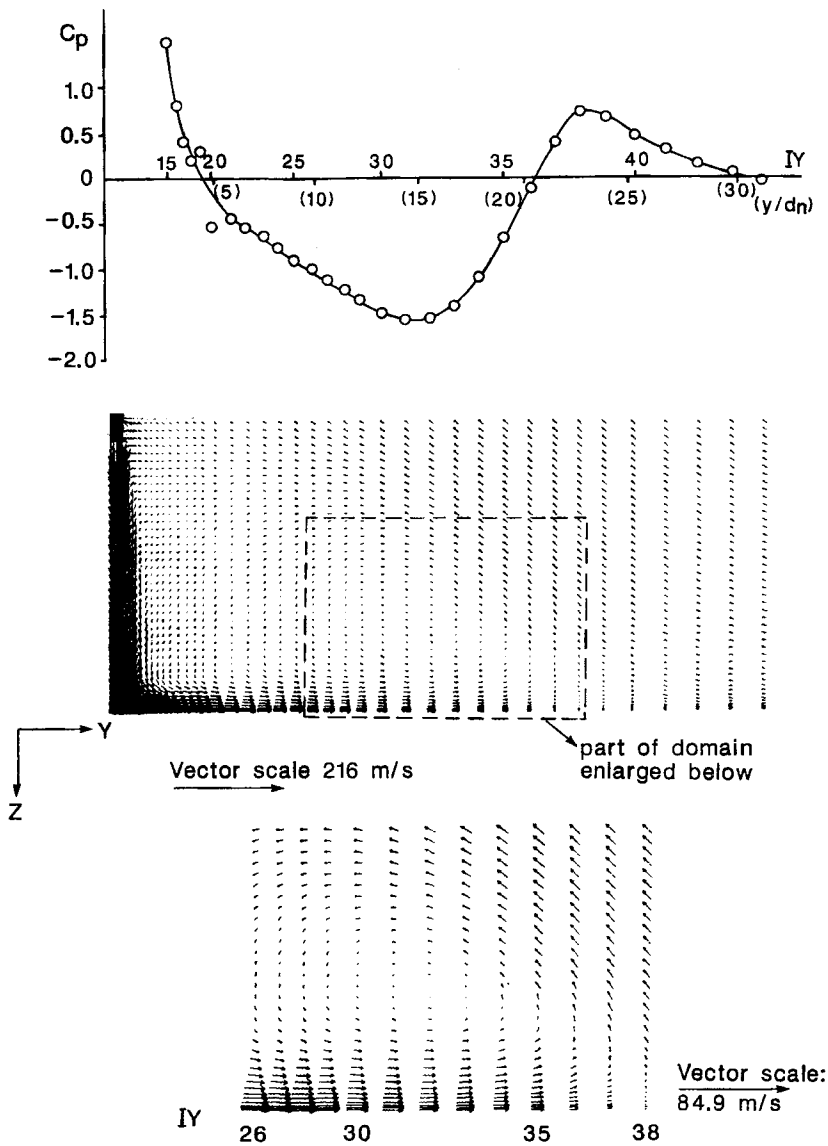


Figure 5. Ground plane C_p plot and velocity vector output for typical numerically modelled impinging jet in cross-flow case

turbulence model will improve this, it is felt to be sufficiently accurate for the present purposes. Increasing nozzle height will, of course, increase the magnitude of these errors and hence the errors in the wall jet initial conditions. For both the free jet and wall jet, however, both the correct specification of turbulence intensity and the extent of the computational domain have been shown to be most important.

The cross-flow calculations have predicted the vortex self-similarity to a reasonably accurate degree. They have also shown the correct trends in terms of ground vortex movement with

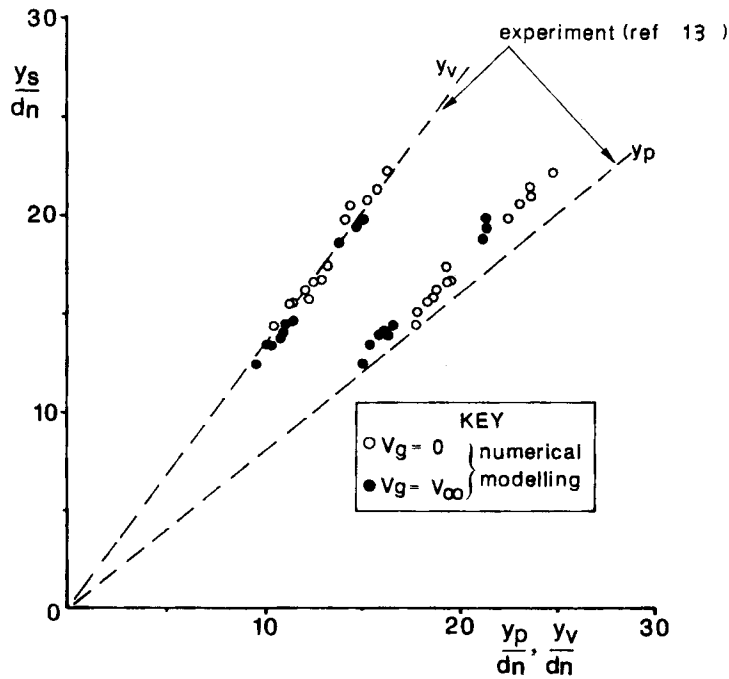


Figure 6. Ground vortex self-similarity—comparison between experiment¹³ and numerical modelling

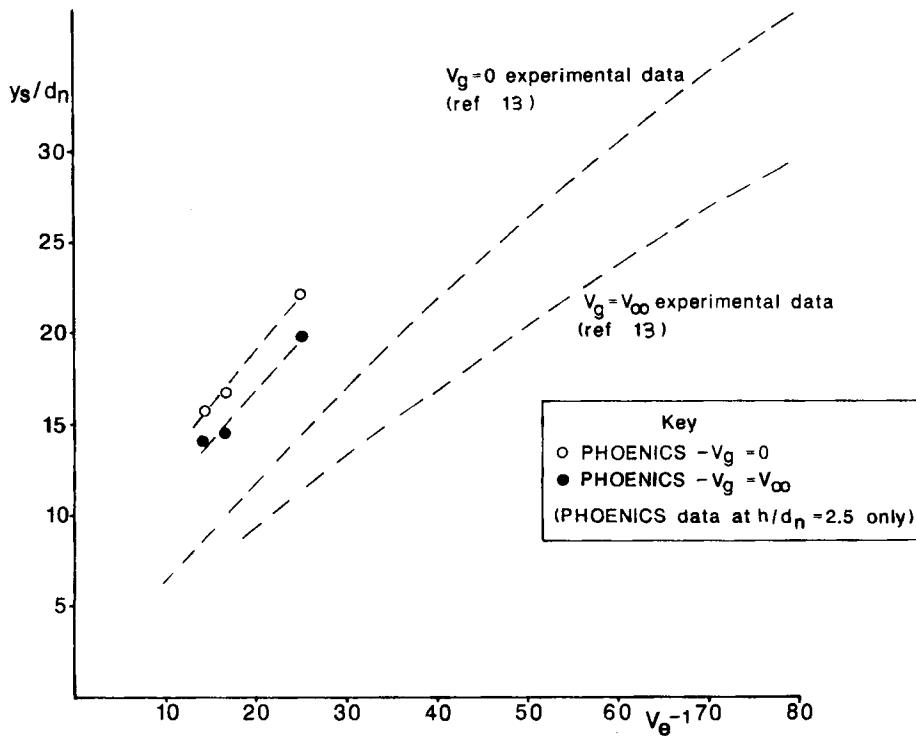


Figure 7. Normalized vortex separation distance against effective velocity ratio—comparison between experiment¹³ and numerical modelling

varying effective velocity ratio and rolling road operation; that is, penetration decreases as free stream velocity increases or jet exit velocity decreases or when the rolling road is used. Vortex separation was overpredicted by about 7 jet diameters in the worst case, this being primarily attributed to the 2D modelling assumptions. The reduction in separation with moving ground plane operation was underpredicted by about 50%.

ACKNOWLEDGEMENTS

The authors wish to thank British Aerospace plc and, in particular, Mr. P. G. Knott and Mr. P. Curtis for their help with the current work.

REFERENCES

1. R. E. Kuhn, 'The induced aerodynamics of jet and fan powered V/STOL aircraft', in A. Krothapalli and C. A. Smith (eds), *Recent Advances in Aerodynamics*, Springer, New York, 1986, pp. 337-373.
2. D. Bray and K. Knowles, 'Normal impinging jet in cross-flow—a parametric study', *AIAA Paper 89-2957, AIAA/ASME/SAE/ASEE 25th Joint Propulsion Conf.*, Monterey, CA, 10-14 July 1989.
3. D. R. Glynn, E. N. Jal and C. M. Milford, 'Numerical prediction of flow entrainment around a V/STOL aircraft in ground effect', *BHRA Seminar and Workshop on Powerful Computing Systems for Fluid Flow Applications*, London, 7-8 June 1988.
4. H. I. Rosten and D. B. Spalding, 'PHOENICS—beginner's guide and user manual', *Concentration Heat and Momentum Ltd., Report No. CHAM TR/100*, 1986.
5. W. Rodi, *Turbulence Models and their Application in Hydraulics—A State of the Art Review*, IAHR, Delft, 1980.
6. D. R. Glynn and E. N. Jal, 'Numerical prediction of flow in free and impinging jets', *Concentration Heat and Momentum Ltd., Report No. CHAM 3181/1*, 1987.
7. M. R. Malin, 'Prediction of radially spreading turbulent jets', *AIAA J.*, **26**, 750-752 (1988).
8. C. P. Donaldson and R. S. Snedeker, 'A study of free jet impingement, Part 1. Mean properties of free and impinging jets', *J. Fluid Mech.*, **45**, 281-319 (1971).
9. P. Curtis, 'Investigation into the behaviour of a single free jet in free air and impinging perpendicularly on the ground', *British Aerospace plc, Report No. BAe-KAD-R-RES-3349*, 1987.
10. M. B. Glauert, 'The wall jet', *J. Fluid Mech.*, **1**, 625-643 (1956).
11. P. Bakke, 'An experimental investigation of a wall jet', *J. Fluid Mech.*, **2**, 467-472 (1957).
12. M. Poreh, Y. G. Tseui and J. E. Cermak, 'Investigation of a turbulent radial wall jet', *J. Appl. Mech.*, **89**, 457-463 (1967).
13. K. Knowles and D. Bray, 'Ground vortex formation with twin jets and moving ground plane', *Procs. 17th Congress Int. Council of the Aeronautical Sciences*, Stockholm, 9-14 September 1990. Paper no. ICAS-90-3.1.2.